ELSEVIER

Physica A 270 (1999) 427–443

PHYSICA A

www.elsevier.com/locate/physa

Diffusional coagulation of superparamagnetic particles in the presence of an external magnetic field

Scarlet Relle[a], Stanley B. Grant[a,*], Costas Tsouris[b]

[a] *Department of Civil and Environmental Engineering, University of California, Irvine, CA 92697, USA*

[b] *Chemical Technology Division, Oak Ridge National Laboratory, P.O.Box 2008, Oak Ridge, TN 37831-6226, USA*

Received 15 September 1998

Abstract

In this paper, we investigate the diffusional coagulation of colloidal superparamagnetic (SP) latex particles that are under the influence of an external magnetic field. The cluster size distributions (CSDs) that evolve with time were determined using an optical set-up that permits the direct visualization of particle clusters. Following the dynamic scaling analysis of van Dongen and Ernst (Phys. Rev. Lett. 54 (1985) 1396), we find that the CSDs all collapse onto a master curve when properly scaled. The bell-shape of this master curve indicates that large clusters preferentially scavenge small clusters in our system. From the time evolution of the average cluster size we infer that the reactivity between large clusters diminishes with increasing cluster size. These results are consistent with a simple mathematical formulation of the coagulation rate constant, or kernel, for the Brownian coagulation of magnetic particles. Moreover, our results support a growing body of evidence that the dynamic scaling theory developed by van Dongen and Ernst is a useful framework with which to study the microscale processes governing particle coagulation.

PACS: 61.43.Hv; 11.10.Jj; 82.70.Dd

Keywords: Diffusion limited coagulation; Colloidal magnetic particle coagulation; Dynamic scaling; Cluster size distributions; Superparamagnetic particles; Single cluster detection

* Corresponding author. Fax: +1-949-824-3672.

E-mail address: sbgrant@uci.edu (S.B. Grant)

0378-4371/99/$ - see front matter
PII: S0378-4371(99)00100-4

Notation

Unit designations:	L = length scale M = mass T = time
a	aggregate collision cross-section radius [L]
B	external magnetic field induction [Tesla]
dB/dz	magnetic induction field gradient [Tesla/L]
$C = 0.31$	proportionality constant relating cluster length to cluster volume [L^2]
d_1	diameter of a primary magnetic particle [L]
D	aggregate diffusion coefficient [L^2/T]
g	gravitational acceleration [L/T^2]
i, j, k	number of constituent particles in an aggregate [-]
$\langle j \rangle = N_1/N_0$	number-average aggregate size [-]
$k_B = 1.38 \times 10^{-23}$	Boltzmann constant [ML^2/T^2 Kelvin]
$K_{11} = 8k_BT/3\eta_v$	kernel for the coagulation of monomers [L^3/T]
K_{ij}	kernel for the coagulation between clusters of magnetic particles containing i and j constituent particles [L^3/T]
l	length of a magnetic aggregate [L]
$N_0(t) = \sum_{j \geqslant 1} n_j(t)$	zeroth moment of magnetic particle size distribution [$1/L^3$]
$N_1(t) = \sum_{j \geqslant 1} jn_j(t)$	first moment of magnetic particle size distribution [$1/L^3$]
$N_0(0)$	initial particle number concentration [$1/L^3$]
n_j	number concentration of magnetic j-mers [$1/L^3$]
r_1	radius of a primary magnetic particle [L]
s(t)	scaling factor [-]
T	temperature [Kelvin]
t	time [T]
V	volume of a magnetic cluster [L^3]

Greek letters

α	positive constant
$\phi = 3.6 \times 10^{-5}$	initial particle volume fraction [-]
γ	exponent relating cluster size to diffusion coefficient [-]
$\eta = j/\langle j \rangle$	scaling variable [-]
η_v	dynamic viscosity [M/LT]
κ	volume magnetic susceptibility [-]
λ	degree of homogeneity of the coagulation kernel [-]
μ	exponent that governs the small i/j limit of K_{ij} [-]

$\tau_B = 2/(K_{11}N_0(0))$	characteristic time scale for the Brownian coagulation of monomers [T]
$\psi(\eta)$	self-preserving cluster size distribution function [-]

1. Introduction

The coagulation of magnetic particles is of importance to a broad array of scientific and practical processes. Examples include magnetic particle separation [1–10], the genesis of magnetism in sedimentary rocks [11,12], magnetic granulometry [11], and the formation and rheology of ferrofluids [13,14], to name a few. All of these processes are strongly influenced by the magnetic properties of the particles involved. Particles with small positive magnetic susceptibility are weakly magnetic, and belong to the paramagnetic and antiferromagnetic groups (i.e., metals and transition elements). On the other hand, particles with large positive magnetic susceptibility contain elements from the ferromagnetic and ferrimagnetic groups (i.e., iron, cobalt, and nickel), and are strongly magnetic. Magnetic properties of the latter group vary significantly with particle size. In the order of decreasing size, magnetic particles are classified as multidomain (MD), single domain (SD), or superparamagnetic (SP) [15]. In general, MD particles have small and unstable remanent magnetism, SD particles possess large and stable remanent magnetism, and SP particles exhibit no magnetic remanence.

Previous investigations of the coagulation kinetics of magnetic particles have focused on the microscale interaction forces that develop between magnetic particles on close approach [16–20], or the dynamic scaling properties of the resulting cluster size distributions [21,22]. Relative to the latter issue, it has been demonstrated numerically [21] and experimentally [22] that as magnetic particles coagulate, the distribution of cluster sizes adopts a self-similar shape, and that the moments of the cluster size distribution obey power-laws of time. The exact shape of the cluster size distribution and the magnitude of the power-law exponents appear to be determined by the transport processes that bring clusters into contact, and the physical and surface-chemical forces that develop on close approach. What is currently not clear, however, is how the magnetic properties of the particles (e.g., their classification as SD, MD, or SP) influence the dynamic scaling properties of the resulting cluster size distributions. As a first step toward addressing this larger question, we experimentally determined the cluster size distributions that arise from the diffusional coagulation of SP particles in the presence of an external magnetic field. These results are interpreted in the context of a simple mathematical model for the diffusional coagulation of strong dipoles, and are compared to previously published results involving the coagulation of non-SP particles.

2. Theory

The equation that describes the coagulation kinetics of colloidal clusters was developed by von Smoluchowski at the turn of the century [23]:

$$\frac{dn_j}{dt} = \frac{1}{2}\sum_{i+k=j} K_{ik} n_i n_k - n_j \sum_{i\geqslant 1} K_{ij} n_i \,. \tag{1}$$

According to this equation, the temporal change in the concentration of clusters containing j primary particles, n_j (LHS), depends on their formation by coagulation of k-mers and i-mers where $i+k=j$ (first term on the RHS), and their loss by coagulation with all other sized aggregates (second term on the RHS). The coagulation rate constant or kernel, K_{ij}, contains information regarding the transport mechanisms which bring about particle–particle contact, and the physicochemical interactions that determine the probability of particle–particle attachment. For colloidal clusters undergoing diffusive coagulation, and when every collision is successful, the coagulation rate constant may be expressed in terms of the Brownian collision frequency function [23]:

$$K_{ij} = 4\pi(D_i + D_j)(a_i + a_j)\,, \tag{2}$$

where D_i and a_i are the diffusion coefficient and collision cross-section, respectively, of a cluster containing i primary particles. This kernel may also describe the diffusive coagulation of colloidal magnetic clusters, subject to two fundamental assumptions: (i) magnetic particles coagulate in a "tip-to-tip" manner forming aggregates with chain-like morphologies and the collision cross-section of magnetic aggregates remains equal to the radius of a primary particle throughout the coagulation process ($a_i = a_j = r_1$) [21,24]; (ii) the diffusion coefficient for particle aggregates decays like a power-law of aggregate size $D_j \sim j^{-\gamma}$ where γ is a positive constant in the range 0 to 1 [21,24]. Given these assumptions, the Brownian kernel describing the coagulation of magnetic clusters can be written exclusively in terms of i and j [21,24]:

$$K_{ij} \sim i^{-\gamma} + j^{-\gamma}\,. \tag{3}$$

According to van Dongen and Ernst (hereafter referred to as VDE) [25], mathematically homogeneous kernels like (3) can be analyzed in terms of two parameters λ and μ:

$$K_{\alpha i,\alpha j} = \alpha^{\lambda}(K_{ij}), \quad \lambda \leqslant 2\,, \tag{4a}$$

$$K_{ij} \sim (i/j)^{\mu} j^{\lambda}, \quad j \gg i, \;\; \lambda \leqslant 1+\mu\,, \tag{4b}$$

where α is some positive constant, λ is the degree of homogeneity of the kernel with respect to arguments i and j, and the exponent μ governs the small i/j limit of K_{ij}. The value of λ indicates whether the reactivity between aggregates of the same size increases ($\lambda > 0$) or decreases ($\lambda < 0$) with aggregate size. The parameter μ indicates whether large aggregates preferentially react with small aggregates ($\mu < 0$),

or coagulation between large aggregates predominates ($\mu > 0$). For the kernel given by Eq. (3) we have the following result:

$$\lambda = \mu = -\gamma < 0 \,. \tag{5}$$

It has been shown theoretically and experimentally that when clusters undergo coagulation, the cluster size distribution function n_j adopts the following dynamic scaling relationship at long times and large j [21,22,26–28]:

$$n_j(t) \sim s^{-2}\psi(j/s) \,. \tag{6}$$

The scaling factor $s(t)$ is related to the number-average cluster size $\langle j \rangle$, and $\psi(\eta)$ represents the shape of the cluster size distribution. The number-average cluster size is the ratio of the first and zeroth moments of the particle size distribution function:

$$\langle j \rangle = \frac{N_1}{N_0} \,. \tag{7}$$

The functional forms of $s(t)$ and $\psi(\eta)$ depend on the mathematical properties of the coagulation kernel (i.e., λ and μ). For kernels like (3) with $\lambda < 1$ and $\mu < 0$, the prediction is that for long times,

$$s(t) \sim \langle j \rangle \sim t^{1/(1-\lambda)} \tag{8}$$

and $\psi(\eta)$ is bell-shaped. The exact relationships between $s(t), \psi(\eta), \lambda$, and μ are summarized elsewhere [26,28].

Our goal in this paper is to experimentally test these predictions for the case where superparamagnetic particles coagulate in the presence of an applied magnetic field.

3. Materials and methods

3.1. Coagulation experiments

Particle coagulation experiments were carried out in the presence of an externally applied magnetic field as illustrated in Fig. 1a. A Model 2V1 magnet purchased from Applied Magnetics Laboratory (Baltimore, MD) was oriented in the vertical direction such that its magnetic force field was parallel to gravity. During the coagulation experiments the power supply to the magnet was turned off, and therefore the magnetic force field was solely the result of the remanent magnetism of the magnet poles. The reactor containing the experimental sample was a micro-rectangular tube, 2 mm $\times$ 100 μm in cross-section, manufactured by Wale Apparatus (Hallertown, PA). The reactor was secured over the magnetic pole of the magnet such that its long axis was also parallel to gravity. The experimental sample consisted of an aqueous suspension of superparamagnetic latex microspheres purchased from Bangs Laboratories (Carmel, IN). According to the manufacturer, the mean diameter and density of these microspheres were 0.89 ± 0.2 μm and 1.155 g/cm^3, respectively. These microspheres were suspended in an aqueous solution (pH 5.6, 0.01 M NaCl) at a final concentration

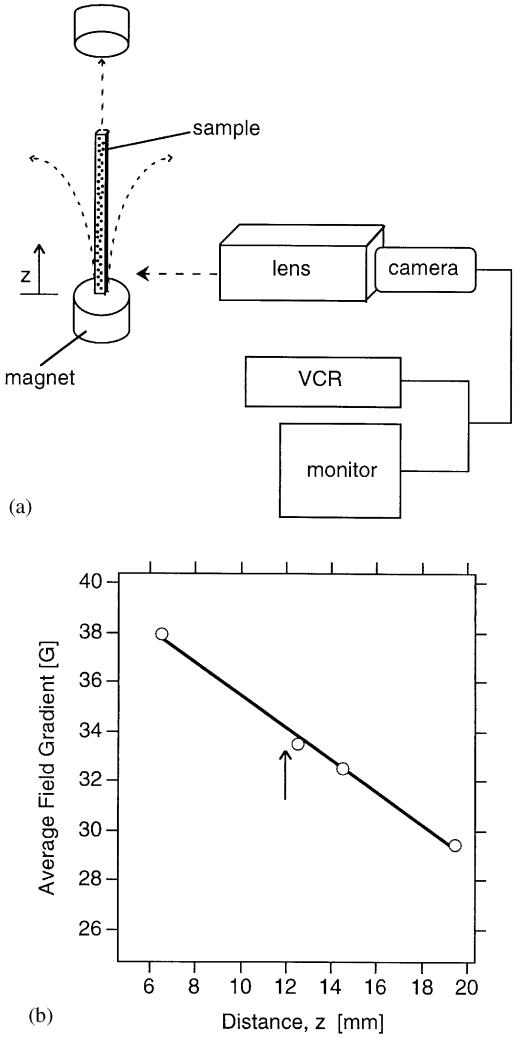

Fig. 1. Block diagram of the experimental system and the optical set-up (panel a). The variation of the external magnetic field strength with increasing distance above the magnetic pole (panel b).

of 1.5×10^8 p/ml ($\phi = 3.6 \times 10^{-5}$), and then loaded into the reactor by capillary action. The Brownian coagulation time scale for these experiments is: $\tau_B = 2/(K_{11} N_0(0)) =$ 20 min. To record the coagulation kinetics of superparamagnetic latex microspheres an optical set-up consisting of a QM-100 250X lens (Questar Corp.; New Hope, PA), a model TC651EA camera (Burle Security products; Lancaster, PA), a Panasonic Video Camera Recorder, and a Panasonic monitor were used. The recorded field of view had dimensions of 479×639 pixels, corresponding to a control volume of 8.6×10^{-5} ml. After the initiation of coagulation, video footage of the particles was recorded at

10 min intervals each for a duration of 5 min. VCR digital images of the aggregates were captured by a Power Macintosh computer, and the length of individual clusters were analyzed using the public domain NIH Image program (developed at the U.S. National Institute of Health and available on the Internet at http://rsb.info.nih.gov/nih-image/).

3.2. Scanning electron microscope

A Philips XL30 scanning electron microscope (SEM) was used to assess the degree of polydispersity of the superparamagnetic (SP) latex particles. From the aqueous stock suspension of the SP particles, an aliquot of 0.1μl was withdrawn with the aid of a micro-pipetter. The fluid was then placed on a 12 mm glass slide that had been previously secured onto an SEM aluminum stub. The sample was air dried in a dust free environment, and subsequently gold coated for SEM observations.

3.3. Photon correlation spectroscopy (PCS)

The mean size of the superparamagnetic latex microspheres was determined by the manufacturer, and verified in our laboratory by measuring their average hydrodynamic diameter using PCS (N4MD Sub-Micron Particle Size Analyzer, Coulter Scientific Instruments). All measurements were conducted in deionized water (Milli-Q, Millipore, Bedford, MA), at a temperature of 23°C, and at a scattering angle of 90°. The reported mean diameter value is the average of 18 measurements taken every 400 s over a period of 2 h.

3.4. Zeta potential measurements

Zeta potential measurements of the super-paramagnetic latex microspheres were conducted using a Lazer-Zee Meter Model 501 (Pen Kem Inc., Bedford Hills, NY). The microspheres were suspended in an electrolyte solution of 0.01 M NaCl (pH 5.6) at a final concentration of 1.5×10^8 particles/ml. The electrolyte solution was prepared from deionized water (Milli-Q, Millipore, Bedford, MA), and analytical-grade NaCl. The reported zeta potential value represents the average of 10 measurements each carried out at a temperature of 23°C.

3.5. Hysteresis loop

Hysteresis loops were obtained for the superparamagnetic latex microspheres using a Vibrating Sample Magnetometer (VSM) located at the Institute for Rock Magnetism, University of Minnesota. A dried particle sample was mounted in the VSM at the end of a rod which vibrated at a frequency of 100 Hz in a uniform magnetic field supplied by an electromagnet. On each side of the mounted sample were two

pick-up coils which generated a voltage proportional to the vibration amplitude, frequency, and magnetization of the sample. Since the amplitude and frequency of the vibration were fixed, the voltage produced was proportional to the magnetic moment of the sample. The magnetic remanence of the sample was measured at zero magnetic field strength, and the coercivity was measured by reversing the direction of the applied magnetic field. The operation of the VSM was controlled by a PC that processed the experimental information, and displayed the results as a plot of magnetization values of the particles as a function of the intensity of the external magnetic field.

4. Results

4.1. Characterization of the magnetic field

A GM1A model GaussMeter (Applied Magnetics Laboratory Inc., Baltimore, MD) was used to measure the variation of the magnetic field strength as a function of increasing distance from the magnetic pole. As illustrated in Fig. 1b, the magnetic field strength decreases in an approximately linear fashion with increasing distance above the magnetic pole. The slope of these data corresponds to a magnetic field gradient of $dB/dz = -0.65 \pm 0.03$ G/mm. The video camera was focused on a point within the reactor 12 mm above the lower magnetic pole (indicated by the arrow in Fig. 1b).

4.2. Characterization of the magnetic particles

The magnetic particles used in this study were carboxylate modified superparamagnetic (SP) latex microspheres purchased from Bangs Laboratories (Carmel, IN). According to the manufacturer, these microspheres have a mean diameter of 0.89 ± 0.2 μm, although scanning electron microscope observations reveal that these microspheres are polydisperse (Fig. 2a). Photon correlation spectroscopy measurements carried out in our laboratory indicate that the particles have a mean diameter of 0.77 ± 0.2 μm. In the subsequent calculations, we have used the mean particle diameter value determined in our laboratory. When received from the manufacturer, the particles were coated with sodium dodecyl sulfate (SDS) and their average ζ-potential was determined to be -46 ± 5 mV. In the absence of an applied magnetic field, the SDS coated particles were stable, presumably due to a combination of electrostatic and steric repulsive forces.

The magnetic character of these particles arises from an even dispersion of crystalline magnetite (11% by weight) within their latex matrix. The hysteresis loop in Fig. 2b indicates that these particles possess virtually no remanent magnetization ($M_r = 658$ nA m^2) and virtually no coercivity ($H_c = 290$ μT), consistent with their classification as superparamagnetic. Following the approach outlined by Promislow et al. [24],

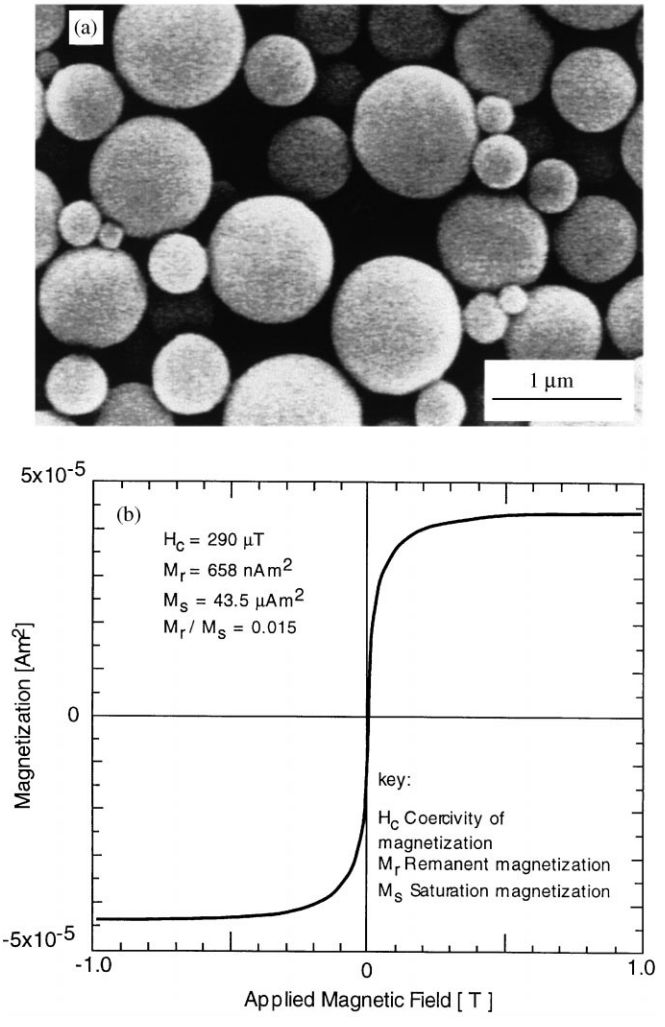

Fig. 2. SEM photograph of the superparamagnetic latex microspheres (panel a), and their hysteresis loop (panel b).

we determined that the effective volume magnetic susceptibility for the particles is $\kappa = 0.6$.

4.3. Characterization of particle size distributions

4.3.1. Estimates of aggregate volume

Video camera images of the coagulation process revealed tip-to-tip aggregation kinetics for the SP particles, and the formation of elongated clusters with chain-like morphologies (see Fig. 3). Throughout the coagulation process, the length of the aggregates

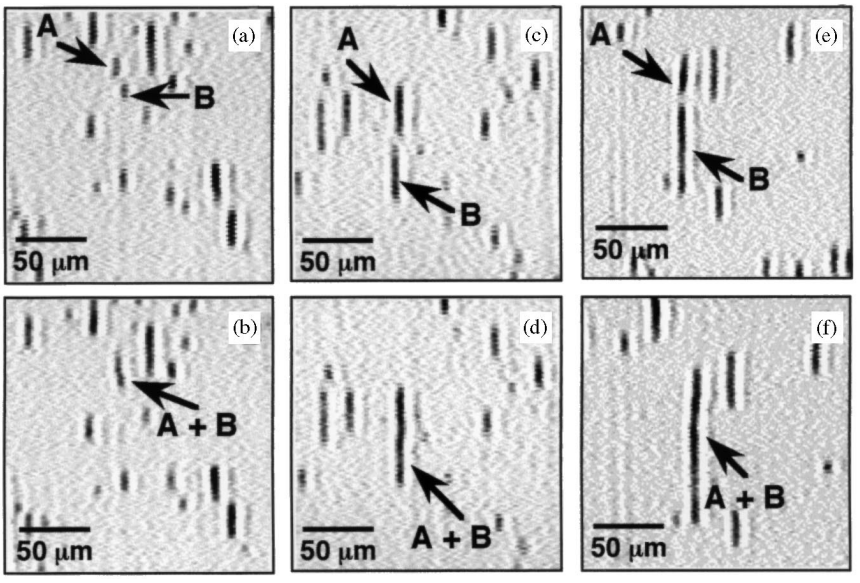

Fig. 3. Video images of three pairs of aggregates with different lengths (upper panels), which coagulated tip-to-tip to form new elongated chain-like clusters (bottom panels).

increased while their width remained equal to, or less than, 1 *pixel*, the resolution limit of our imaging technique. At the magnification used, 1 *pixel* is equivalent to a distance of 1.68 μm, or approximately two average particle diameters ($\approx 2d_1$). To estimate the volume of each aggregate, we assumed that the aggregate volume V varies directly with its length l, such that $V = Cl$, where l is measured by the NIH Image Program (see Section 3). The numerical value of the proportionality constant C is calculated from the expression for the initial particle volume fraction, $\phi = ClN_1(0) = 3.6 \times 10^{-5}$, and it is found to be equal to 0.31. It is important to note that the only critical assumption here is that the aggregate width remains constant during the course of the coagulation process; the exact numerical value of C is of no significance to our subsequent analysis.

To assess the accuracy of this approach, we examined if our estimated volumes obeyed conservation of particle volume. This was accomplished by identifying several coagulation events on the video clips, and then determining the volume of the particle clusters before and after coagulation. Fig. 3 shows three pairs of aggregates with different lengths (upper panels) that coagulated tip-to-tip to form new elongated clusters (lower panels). We noticed that immediately after two clusters joined, the length of the new cluster increased and decreased in an oscillatory manner, until at some point in time a stable length was achieved. This oscillation is presumably due to rearrangement of particles within the newly formed cluster, and will be a topic of future study. For the coagulation events illustrated in Fig. 3, the volume of the clusters identified as A, B and $A + B$ were estimated from at least five video frames using the protocol described

Table 1
Calculated volumes of magnetic clusters

Panels[a]	V_A[b] (μm^3)	V_B[b] (μm^3)	$V_A + V_B$ (μm^3)	V_{A+B}[c] (μm^3)
a,b	4.77 ± 0.63	3.95 ± 0.47	8.71 ± 0.92	7.74 ± 0.66
c,d	12.19 ± 0.59	12.39 ± 0.49	24.58 ± 0.89	21.52 ± 2.03
e,f	10.59 ± 0.32	26.15 ± 0.41	36.74 ± 0.73	36.28 ± 1.09

[a]Refer to the set of panels in Fig. 3.
[b]Estimated volume of clusters A or B before aggregation.
[c]Estimated volume of cluster A+B after aggregation.

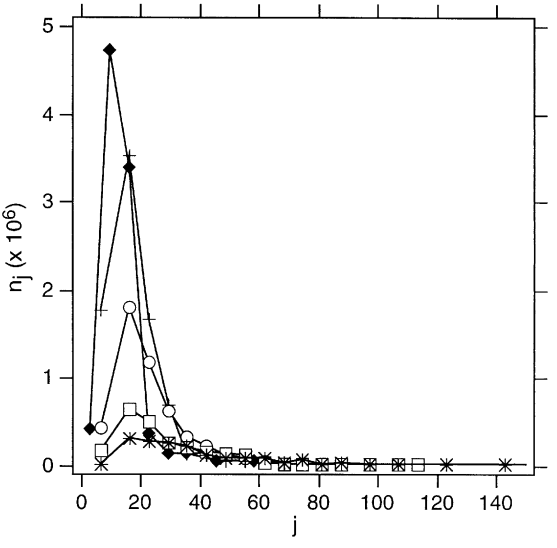

Fig. 4. Cluster size distributions (CSDs) measured at different times after the onset of coagulation: 10 (diamonds), 30 (crosses), 60 (open circles), 120 (open squares), and 300 (asterisks) minutes.

above, and the resulting average volumes and standard deviations are summarized in Table 1. To within experimental error, the summed volumes of the clusters A and B before aggregation ($V_A + V_B$) is equal to the volume of the clusters $A + B$ formed after aggregation (V_{A+B}). Hence, our method for estimating cluster volume appears to conserve particle volume, at least over the short period of time encompassed by the coagulation events shown in Fig. 3.

4.3.2. Cluster size distributions

Using the method described above to estimate aggregate volume, we computed cluster size distributions (CSDs) for the SP clusters after $10, 30, 60, 120$, and 300 min of coagulation (Fig. 4). As time progresses, the concentration of the small aggregates declines, and the cluster size distribution shifts toward longer chain lengths.

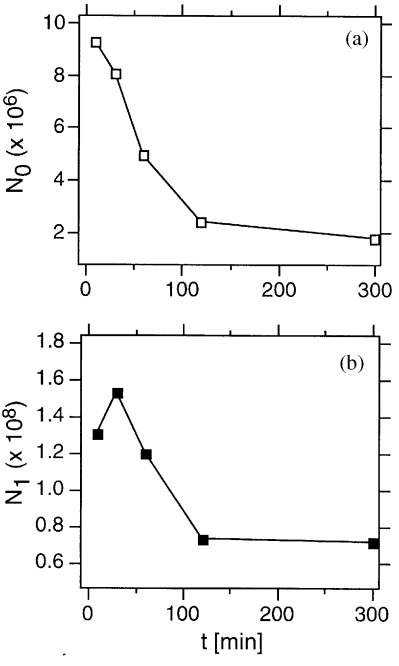

Fig. 5. The variation in the zeroth moment N_0 (panel a) and the first moment N_1 (panel b) of the cluster size distribution function.

4.3.3. Moments of cluster size distributions

The zeroth and first moments of the CSDs were numerically computed and are plotted against time in Fig. 5. As the magnetic particles become progressively more clustered, the concentration of total clusters (as indicated by N_0) and the concentration of total primary particles (as indicated by N_1) both decline with time. The reported N_0 values should be highly accurate because no significant assumptions are invoked in their calculation: They are determined simply by counting the number of aggregates present at any time in the imaged volume. On the other hand, the N_1 values depend on accurately measuring the volume of each individual aggregate present in the imaged volume. As mentioned earlier, our method for estimating volume assumes that the aggregates maintain a constant width as they cluster, while in practice the width of the aggregates appeared to grow slightly with time. Indeed, the 50% decrease in N_1 that occurs between 30 min and 2 h could be fully accounted for if the average width of the aggregates increased from one to two average-sized particles over the same time period – a change that could not have been quantified by our experimental set-up. In summary, the values of N_0 are an accurate measure of the total cluster concentration in our system, and N_0 declines with time as the system becomes more clustered. The values of N_1 also decline with time after 30 min, which may be the result of some physical process (e.g., a net loss of particles from the visualized volume by sedimentation) or, possibly, because the width of the clusters increases with

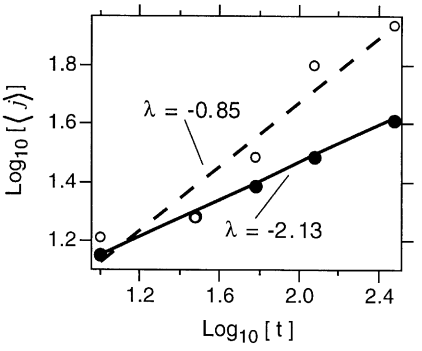

Fig. 6. Log-log plot of the average aggregate size $\langle j \rangle$ vs. time t utilizing either experimentally determined N_1 values (filled circles) or a constant N_1 value (open circles). The solid and the dashed lines represent best fit lines for the two data sets. The reported λ values were calculated from the slopes of the lines (see Eq. (8)).

time, contrary to our assumption that the volume of a cluster is proportional to its length.

4.3.4. Estimates of the homogeneity constant λ

If the scaling relationships presented in the Theory section apply to our system, then we should be able to estimate the homogeneity constant λ from our data. Eq. (8) predicts that a logarithmic plot of $\langle j \rangle = N_1/N_0$ versus t should yield a straight line with a slope equal to $1/(1-\lambda)$. Because there is some question regarding our experimental estimates of N_1 (see last section), we carried out this analysis in two ways, by (i) utilizing the N_1 values estimated directly from the CSDs, and (ii) utilizing a constant N_1 value equal to the initial particle number concentration, 1.5×10^8 p/ml. In the former case, we are assuming that our volume estimation technique is accurate, while in the latter case we are assuming that the decline observed in the value of N_1 (see Fig. 5b) is an artifact of our data reduction method. The resulting plots of $\langle j \rangle$ vs. t are shown in Fig. 6. If we assume that N_1 is constant (open circles in Fig. 6), we obtain a slope that corresponds to $\lambda = -0.85$. On the other hand, if we utilize the experimentally determined values of N_1 (solid symbols) the result is $\lambda = -2.13$. Because these two estimates represent extreme limits for our system, we conclude that the value of λ is bracketed as follows: $-2.13 \leqslant \lambda \leqslant -0.85$. The upper-limit value for λ ($= -0.85$) is in quantitative agreement with the Brownian kernel for the coagulation of magnetic particles (see Eqs. (3) and (5)), and previous estimates of the parameter γ ($=0$ to 1). A negative value of λ indicates that the reactivity between magnetic clusters of the same size declines with cluster size.

4.3.5. Dynamic scaling of the CSDs

According to scaling theory, the measured CSDs should all collapse onto a "master" curve if they are replotted as $n_j(t)/s(t)^{-2}$ versus $j/s(t)$, where $s(t) = \langle j \rangle = N_1/N_0$

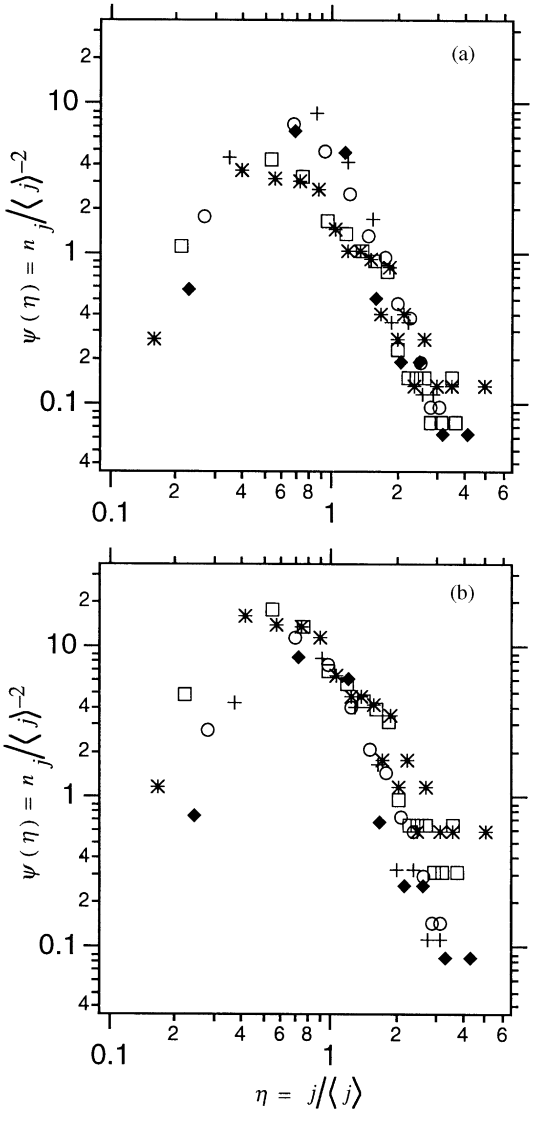

Fig. 7. Dynamic scaling of the measured CSDs utilizing experimentally determined N_1 values (panel a), or a constant N_1 value (panel b). The symbols are defined in the legend for Fig. 4.

(see Eqs. (6) and (7)). As illustrated in Fig. 7a, this expectation is fulfilled, and the shape of the master curve ψ is bell-shaped. The bell-shape of the scaling function ψ is consistent with the preferential coagulation between small and large clusters. In terms of the VDE analysis, these results imply that $\mu < 0$. We repeated the scaling analysis by multiplying each of the CSDs by a constant factor chosen so that the value of N_1 would remain constant ($=1.5 \times 10^8$ p/ml) over the entire course of the experiment. Using this second approach, the transformed CSDs also collapse onto a

bell-shaped master curve (Fig. 7b). Hence, the general bell-shape of ψ is not sensitive to assumptions regarding the constancy of N_1.

5. Discussion

For the system studied here, the CSD evolved to a self-similar bell-shaped form implying that $\mu < 0$, and the average cluster size increased as a power law of time with an exponent consistent with $\lambda < 0$. In the presence of an external magnetic field, SP latex microspheres become magnetized, and form elongated magnetic clusters oriented in the direction of the external magnetic field. These magnetic clusters can be thought of as small bar magnets that attract one another, and also experience an attraction for the external magnetic pole. The presence of the external magnetic field defines their orientation in space, and hinders their Brownian diffusion. This phenomenon has been discussed theoretically by Wilhelm [29] and qualitatively by Promislow et al. [24]. As magnetic clusters grow and develop into stronger bar magnets with large dipole moments, they become more susceptible to the controlling nature of the external magnetic field. Aggregate diffusivity also decreases with increasing size. These two factors result in a reduced collision frequency and, in turn, diminished reactivity between large clusters (i.e., $\lambda < 0$). On the other hand, the diffusivity of small magnetic clusters is restrained to a lesser extent by the presence of the external magnetic field. The smaller clusters diffuse more freely, make more frequent contacts with other aggregates, and coagulate readily with large magnetic clusters with strong dipole moments. The result is the preferential coagulation of small and large aggregates, and $\mu < 0$.

The Brownian kernel presented in the Theory section Eq. (3) is characterized by $\lambda = \mu < 0$, which is qualitatively consistent with the data reported in this study. However, the extent to which equation 3 models the coagulation of magnetic clusters may depend on the strength of the external magnetic field, and the nature of the magnetic particles. For particles with remanent magnetism (e.g., MD and SD particles) and if the external magnetic field is sufficiently weak, particle coagulation is driven primarily by the remanent magnetization of the particles. In this case, as aggregates grow in size their mobility decreases and, importantly, their capture radius *increases* because they become larger and stronger magnets. This could lead to a situation where the reactivity between aggregates increases with increasing aggregate size (i.e., $\lambda > 0$), contrary to our mathematical formulation of the coagulation kernel (equation 3 with $\gamma < 0$) and the experimental results reported here. Indeed, Helgessen et al. [22] studied the aggregation of magnetic microspheres with remanent magnetization, and found that $\lambda = 0.4$ and $\lambda = 0.3$ for the coagulation of colloidal magnetic particles with large and small remanent magnetizations, respectively. Consequently, for non-SP particles it may be necessary to modify the coagulation kernel to take into account the effects of dipole–dipole and dipole–field interactions. This has been attempted by Wilhelm [29] in his mathematical derivation of the diffusional coagulation kernel for colloidal magnetic particles.

6. Conclusion

We employed an image analysis technique to determine the experimental cluster size distributions that result from the diffusive coagulation of SP latex microspheres in the presence of an external magnetic field. Dynamic scaling analysis of these data revealed that the CSDs collapse onto a bell-shaped master curve, consistent with the preferential binding between large and small clusters ($\mu < 0$). Furthermore, we found that the average cluster size, determined by the ratio of first to zeroth moments of the CSDs, increased as a power-law of time with an exponent consistent with $\lambda < 0$. The fact that λ is negative for our system is probably a consequence of the orienting nature of the external magnetic field which limits the diffusivity of large clusters. Furthermore, the fact that both μ and λ are less than zero is qualitatively consistent with a simple formulation of the kernel for the diffusional coagulation of colloidal magnetic particles. On the other hand, the coagulation kinetics of particles with remanent magnetization appears to be characterized by $\lambda > 0$, perhaps due to the dipole–dipole interactions that occur between large clusters in those cases. To accurately describe the coagulation kinetics for particles with remanent magnetism, a kernel must be employed that includes both dipole–field and dipole–dipole interactions. Overall, these results are further evidence that dynamic scaling analysis can be successfully employed to probe the physical mechanisms responsible for particle coagulation.

Acknowledgements

Support for this work was provided to SBG by an NSF Career Award (BES-9502493), and to CT by the Division of Chemical Sciences, Office of Basic Energy Sciences, U.S. Department of Energy. The authors would like to thank the Institute for Rock Magnetism (IRM) at the University of Minnesota for hosting SR as a Visiting Student Fellow. Jim Marvin, Mike Jackson, and Bruce Moskowitz at the IRM are thanked for guidance and stimulating discussions. Some of the experiments were conducted at the Oak Ridge National Laboratory, which is managed by Lockheed Martin Energy Research Corp. under contract DE-AC05-96OR22464 with the U.S. Department of Energy.

References

[1] G. Bitton, O. Pancorbo, G.E. Gifford, Water Res. 10 (1976) 978.
[2] C. De Latour, IEEE Trans. Magn. 9 (1973) 314.
[3] C. De Latour, H. Kolm, IEEE Trans. Magn. 11 (1975) 1570.
[4] P. Anad, J.E. Etzel, F.J. Friedlander, IEEE Trans. Magn. 21 (1985) 2062.
[5] G. Bitton, R. Mitchell, Water Res. 8 (1974) 107.
[6] L. Petrakis, P. Ahner, IEEE Trans. Magn. 14 (1978) 491.
[7] L. Nunez, B.A. Buchholz, G.F. Vandergrift, Separation Sci. Technol. 30 (1995) 1455.
[8] K. Harding, W. Baxter, IEEE Trans. Magn. 17 (1981) 2795.

[9] J. Ugelstad, A. Berge, J. Ellingsen, R. Bjorgum, R. Schmid, P. Stenstad, O. Aune, T.N. Nilsen, S. Funderud, K. Nustad, Future Directions in Polymer Colloids, NATO ASI Ser. E: Applied Sciences, vol. 138, Kluwer Academic Publishers, Hingham, MA, 1987, p. 355.
[10] P.A. Munro, P. Dunnill, M.D. Lilly, IEEE Trans. Magn. 5 (1975) 1573.
[11] P.N. Shive, Earth Planetary Sci. Lett. 72 (1985) 117.
[12] G.L. Anson, K.P. Kodama, Geophys. J. Roy. Astron. Soc. 88 (1987) 673.
[13] M.I. Shliomis, Sov. Phys.-Usp. 17 (1974) 153.
[14] R.W. Chantrell, A. Bradbury, J. Popplewell, S.W. Charles, J. Appl. Phys. 53 (1982) 2742.
[15] C. Hunt, B.M. Moskowitz, S. Banerjee, Rock Physics and Phase Relations, A Handbook of Physical Constants, AGU Reference Shelf 3, American Geophysical Union, 1995.
[16] M.R. Parker, R.P.A.R. van Kleef, H.W. Myron, P. Wyder, IEEE Trans. Magn. 18 (1982) 1647.
[17] J. Svoboda, IEEE Trans. Magn. 18 (1982) 796.
[18] C. Tsouris, T.C. Scott, J. Colloid Interface Sci. 171 (1995) 319.
[19] R.A. Williams, X. Jia, Int. J. Mineral Process. 33 (1991) 175.
[20] S. Yiacoumi, D.A. Rountree, C. Tsouris, J. Colloid Interface Sci. 184 (1996) 477.
[21] S. Miyazima, P. Meakin, F. Family, Phys. Rev. A 36 (1987) 1421.
[22] G. Helgesen, A.T. Skjeltorp, P.M. Mors, R. Botet, R. Jullien, Phys. Rev. Lett. 61 (1988) 1736.
[23] M. von Smoluchowski, Phys. Chem. 92 (1917) 129.
[24] J.H.E. Promislow, A. Gast, M. Fermigier, J. Chem. Phys. 102 (1995) 5492.
[25] P.G.J. van Dongen, M.H. Ernst, Phys. Rev. Lett. 54 (1985) 1396.
[26] A. Fernandez-Barbero, A. Schmitt, M. Cabrerizo-Vilchez, R. Martinez-Garcia, Physica A 230 (1996) 53.
[27] M.L. Broide, R.J. Cohen, Phys. Rev. Lett. 64 (1990) 2026.
[28] M.L. Broide, R.J. Cohen, J. Colloid Interface Sci. 153 (1992) 493.
[29] H.E. Wilhelm, Phys. Fluids 29 (1986) 1441.